

Ti Foil Supported Three-Dimensional Porous Silver Film as a High Performance Catalyst for Hydrazine Electrooxidation in KOH Solution

Ran Liu^{1,*}, Jinling Yin², Dianxue Cao²

¹ Department of Chemistry, School of Food Engineering, Harbin University, Harbin, 150086, P.R.China

² Key Laboratory of Superlight Materials and Surface Technology of Ministry of Education, College of Materials Science and Chemical Engineering, Harbin Engineering University, Harbin, 150001, P.R.China

*E-mail: liuran7907@163.com

Received: 17 May 2017 / Accepted: 30 September 2017 / Published: 12 November 2017

An efficient electrocatalyst for hydrazine electrooxidation is beneficial for elevating the cell performance of direct hydrazine fuel cells (DHFCs). Electrocatalysts with a highly porous structure have been extensively studied in the field of electrochemistry, owing to their large catalytically active area and favorable mass transfer. Therefore, in this thesis, a one-step galvanostatic electrodeposition method related to the hydrogen evolution reaction is adopted to deposit a porous silver film on Ti foil (Ag/Ti). Electrochemical measurements are introduced to estimate the ability of the resultant Ag/Ti electrode to catalyze hydrazine electrooxidation. Ag/Ti displays an evident peak at approximately -0.2 V due to hydrazine electrooxidation. The correspondent peak current density reaches 7.7 mA cm⁻² in 0.02 M N₂H₄·H₂O and 1.0 M KOH. This good electrocatalytic capacity may have a bearing on the micropore structure, which offers facile access of the electrolyte to the Ag/Ti surfaces and enables gases to diffuse away from the electrode surfaces promptly to vacate the activated sites.

Keywords: Silver; Porous film; Electrodeposition; Hydrazine electrooxidation

1. INTRODUCTION

A proton exchange membrane fuel cell (PEMFC) using pure hydrogen as anode fuel is treated as the fuel cell with the most desirable prospects, because it possesses high energy density, operates at low temperature and does not face the problem of the electrolyte leakage [1]. However, the high cost and danger associated with transport and storage of pure hydrogen restrict the development of PEMFCs [2]. For the above reasons, alcohols (methanol, ethanol and ethylene glycol) [3-5], formic

acid [6], sodium borohydride [7], hydrogen peroxide [8] and hydrazine [9] can replace pure hydrogen as the anode fuel for fuel cells.

The superiority of hydrazine used as anode fuel for direct hydrazine fuel cells (DHFCs) is mainly manifested in the following aspects [10-12]: (1) Hydrazine is electrooxidized in alkaline medium to form only nitrogen and water and no emission of greenhouse gases occurs. Therefore, DHFC can achieve a zero emission. (2) When hydrazine is electrooxidized in basic solution, no intermediates that can bring about a decrease of the catalyst activity are present, ensuring prolonged catalyst activity and lifetime of DHFC. (3) Compared to direct methanol fuel cells, the theoretic electromotive force for DHFCs is much higher.

Anode catalyst is regarded as an important factor that affects the properties of DHFCs. According to the literatures reported previously, a number of metal materials, including noble metals (Pt, Pd, Au and Ag) [13-16] and transition metals (Ni, Co and Cu) [17-19], have been utilized as the anode catalysts for DHFCs. Among these metals, Ag, as the cheapest precious metal, is usually applied to catalyze hydrazine electrooxidation [20-24]. This is because that Ag has high electrical conductivity, steady physicochemical properties and can exist stably in base solution. For instance, Dong et al. [20] fabricated a Ag/SnO₂ catalyst through a two-step approach, which involved the synthesis of SnO₂ via a solvothermal method, followed by the preparation of Ag/SnO₂ via a chemical reduction method. The resultant Ag/SnO₂ displayed good catalytic performance with a peak potential of -0.12 V vs. SCE. He et al. [21] prepared a reduced graphene oxide (RGO) supported Ag catalyst and used it as the electrocatalyst to catalyze hydrazine electrooxidation. The electrochemical results indicated that the Ag/RGO catalyst showed a high catalytic activity.

Hydrazine electrooxidation occurs at the solid-liquid interface, accompanied by the formation of gas. In view of the characteristic of hydrazine oxidation reaction, the anode catalyst must have a large catalytically active area and favorable mass transfer. Recently, porous materials have stimulated the interest of scientific researchers and have been used extensively in fuel cells [25], lithium ion batteries [26], super capacitors [27] and biosensors [28]. The precious porous structure can enhance the catalyst surface area, provide many more active sites and a pathway for the access of hydrazine to the sample surfaces and accelerate the rate of the electrolyte-electrode interface reaction. Therefore, herein, we attempted to prepare a silver catalyst with a porous structure and apply it as the anode catalyst for DHFC.

It is essential to synthesize a 3D porous electrode via a simple and shape-controlled method. Shin et al. [29,30] created an original template method for fabricating 3D porous materials. At the cathode, the electrochemical reduction reaction of metal ions and hydrogen evolution reaction occur simultaneously. The electrodeposition of metal can only occur in the interspace of hydrogen bubbles and a 3D porous structure is formed. Hydrogen bubbles template method overcomes the disadvantages existed in a traditional template method such as the complexity of preparation and elimination of template and expensive cost.

In a general way, the conventional electrode preparation process is as follows: catalyst powder is uniformly mixed with binder to form a suspension, and then the suspension is coated on a current collector. The weakness of this electrode lies in the low catalyst utility and electrical conductivity, as introducing polymer binder may prevent some catalysts from accessing the electrolyte. So, in this

paper, we directly electrodeposited a porous silver film on the surface of a Ti foil substrate employing hydrogen bubbles as template, to which no polymer binder or surfactants were added. The reason for selecting Ti foil as the substrate is that it can exist stably in alkaline hydrazine electrolyte for long periods and owns the characteristics of light-weight [31]. The resultant Ag/Ti electrode with a porous structure was electrocatalytically active for the oxidation of hydrazine in base solution.

2. EXPERIMENTAL

2.1. Synthesis of Ag/Ti

Galvanostatic deposition was applied to electrodeposit a porous silver film on Ti foil in 0.015 M silver sulfate, 1.5 M potassium thiocyanate and 2 M ammonium chloride [32]. The porous Ag/Ti electrode was prepared with an electrodeposition current of -2 A cm^{-2} and electrodeposition time of 40 s at ambient temperature. The preparation process was accomplished in a three-electrode equipment, including a working electrode (Ti foil, nominal planar area = 1 cm^2), a commercial Ag/AgCl (saturation solution of KCl) reference electrode, and a counter electrode (Pt plate, nominal planar area = 2 cm^2), using an Autolab PGSTAT302 workstation. Before depositing the silver film, Ti foil was first degreased via ultrasonic washing in acetone for 15 min, then immersed in a 50 mL mixed solution composed of 25 mL water, 20 mL nitric acid and 5 mL hydrofluoric acid for several seconds to eliminate surface oxide, then the material was washed with water and vacuum-dried.

2.2. Materials characterization

X-ray diffraction (XRD) information for the sample powder was acquired from a Rigaku D/max-2600/PC diffractometer. A scanning electron microscopy (SEM, HITACHI SU-70) in conjunction with energy dispersive X-ray spectrometer (EDX, BRUKER) was adopted to characterize the surface morphology of the sample.

2.3. Electrochemical tests

Electrochemical tests were completed in the same three-electrode system using the synthesized Ag/Ti electrode as the working electrode. Electrochemical impedance spectroscopy (EIS) was measured in 100000 Hz - 0.01 Hz frequency region and the sinusoidal voltage amplitude was set to 5 mV. Before the electrochemical tests, the porous Ag/Ti electrode was repetitively scanned at 50 mV s^{-1} between -1.2 V and 0.8 V in 1.0 M KOH until the cyclic voltammetric curve became stable. The current densities were gained by normalizing to the nominal planar area of the porous Ag/Ti electrode. The potential given in the thesis was with reference to the Ag/AgCl (saturated solution of KCl) reference electrode. All tests were conducted at ambient temperature unless otherwise stated.

Gas collection tests were achieved in the same three-electrode system as above. By applying fixed current densities from 50 mA cm^{-2} to 250 mA cm^{-2} at intervals of 50 mA cm^{-2} to the system in

0.02 M $N_2H_4 \cdot H_2O$ + 1.0 M KOH and collecting the volume of gas generated from N_2H_4 oxidation in 1 h through the drainage approach, the gas generation rate at each current density was obtained.

3. RESULTS AND DISCUSSION

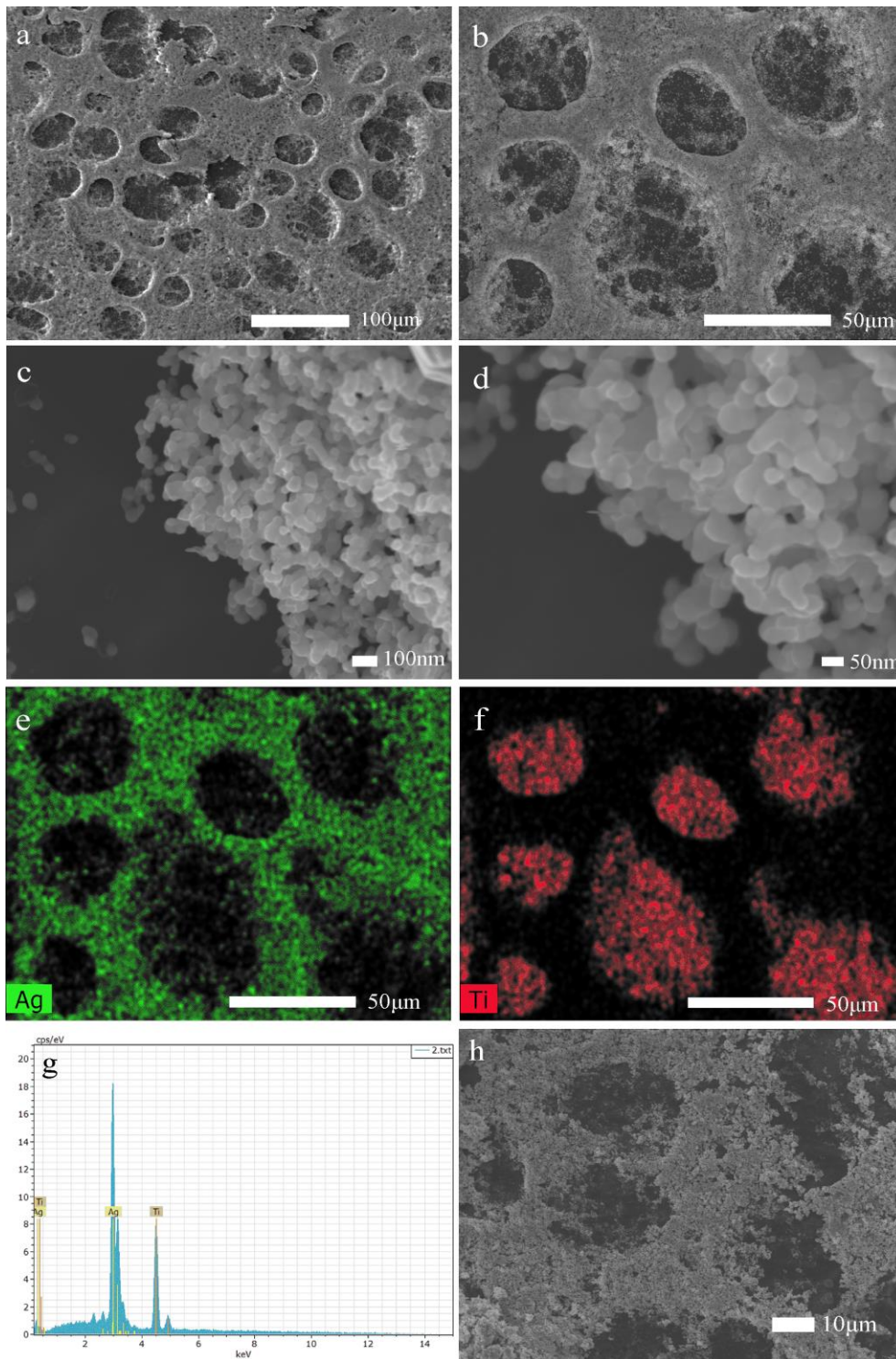


Figure 1. SEM photographs of the sample at various magnifications (a-d), corresponding mapping of Ag and Ti elements from the Ag/Ti displayed in panel b (e-f), EDX spectrum of the Ag/Ti sample (g) and SEM photograph of the Ag/Ti sample after cyclic voltammetry (h).

The SEM photographs of Ag/Ti at various magnifications are given in Figure 1a-d. As seen from Fig. 1a-b, the fabricated silver electrode owns a 3D porous structure and the pore shows an ellipsoid shape. A pore size between 20 μm - 60 μm was observed. Fig. 1c-d exhibit the magnified SEM photograph of the pore walls. As observed, Ag particles with the dimensions ranging from 50 nm to 90 nm are interconnected into a 3D structure. Fig. 1e-f display the correspondent mapping of Ag and Ti elements from Ag/Ti displayed in panel b. As seen, the distribution of Ag is porous-like and has the same counter as the appearance of Ag/Ti, indicating that Ag is distributed homogeneously and fully on Ti foil surfaces. EDX analysis (Fig. 1g) indicated that Ag/Ti is made up of Ag and Ti elements. The intensive peak for elemental Ag revealed the high loading of Ag. The peak for elemental Ti was ascribed to the Ti substrate. Fig. 1h displays the SEM photograph of the Ag/Ti sample after cyclic voltammetry. As seen, the sample still exhibits a porous structure after electrochemical measurement. However, the obvious pore wall collapse can be seen from Fig. 1h.

To guarantee that the prepared silver film contained no impurities, an XRD test was carried out. The as-prepared sample was first dried under vacuum, then the sample powder was scraped off from the Ti substrate to carry out the XRD test for eliminating the effect of the Ti substrate, displayed in Figure 2. Four sharp peaks appeared at 38.04°, 44.24°, 64.42° and 77.4° are assigned to (111), (200), (220) and (311) planes of silver (JCPDS 04-0783). Meanwhile, peaks of substances such as Ag₂O and AgO were not observed in the experimental pattern. The experimental data indicated that Ag particles with a face-centered cubic phase were electrodeposited on the Ti substrate.

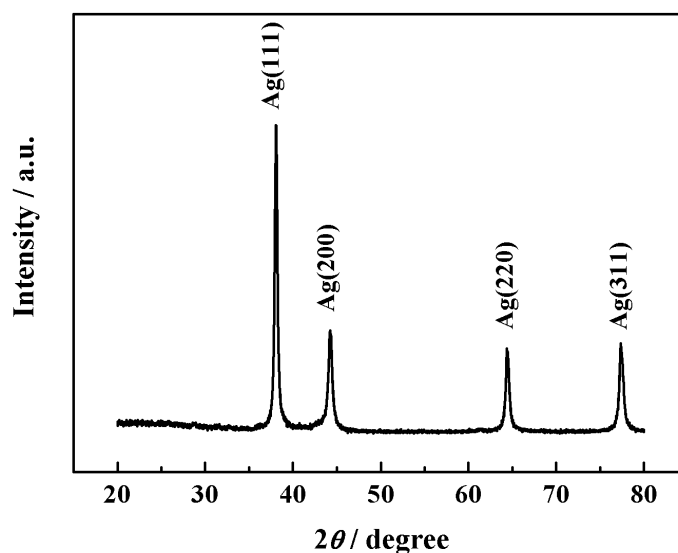


Figure 2. XRD spectrum of the sample powder.

Figure 3 presents the cyclic voltammetric behaviors obtained on the porous Ag/Ti sample in 1.0 M KOH without and with 0.02 M N₂H₄·H₂O at 10 mV s⁻¹. There was no existence of pronounced oxidation peak or reduction peak in KOH electrolyte, indicating that the conversion of silver to low-valence or high-valence silver oxide cannot occur under the potential of -0.8 V ~ 0 V. After the addition of a proper amount of hydrazine, an evident peak occurred at approximately -0.2 V, which

belongs to hydrazine electrooxidation on the Ag/Ti electrode. The correspondent peak current density reached 7.7 mA cm^{-2} . To validate whether the Ti substrate can catalyze hydrazine electrooxidation, a cyclic voltammogram for the Ti substrate in $0.02 \text{ M N}_2\text{H}_4\cdot\text{H}_2\text{O} + 1.0 \text{ M KOH}$ was tested, presented in Fig. 3 inset. Obviously, Ti substrate displayed no electrocatalytic activity with regard to hydrazine electrooxidation, showing that Ag is the electrocatalytic active species. In addition, the electrocatalytic performance for hydrazine electrooxidation on the synthesized Ag/Ti sample is superior than that on some other Ag catalysts reported in the literatures [20,24,33]. For instance, a Ag/SnO₂ catalyst displayed an oxidation peak potential of -0.12 V (vs. SCE) and the correspondent oxidation peak current of $210 \text{ }\mu\text{A}$ in $0.02 \text{ M N}_2\text{H}_4\cdot\text{H}_2\text{O}$ and 1 M KOH at 20 mV s^{-1} [20]. For a Ag/poly ortho-toluidine/modified carbon paste electrode, an oxidation peak occurred at -0.05 V (vs. Ag/AgCl) with a corresponding peak current of $410 \text{ }\mu\text{A}$ in $0.02 \text{ M N}_2\text{H}_4 + 0.1 \text{ M NaOH}$ at 10 mV s^{-1} [33].

Luo and the cooperators [34], Kunal and the cooperators [35] and Nørskov and the cooperators [36] have elucidated that Ag binds too weakly with lots of species (e.g., OH and H). However, it has been proved that surface metal atoms which are located at activated sites participate in surface electrocatalysis process. Ahern et al. [37] proposed that the difference existed in the onset potential of aldehyde electrooxidation and hydrazine electrooxidation on Ag electrode in basic medium can be ascribed to their different activated site mediators. In comparison with aldehyde, hydrazine is electrooxidized at a more positive potential where $\text{Ag}(\text{OH})_{\text{ads}}^*$ is involved. The coverage degree of $\text{Ag}(\text{OH})_{\text{ads}}^*$ species on the catalyst surfaces is relevant to activated nature of catalyst surface. The high electrocatalytic capability of the Ag/Ti sample can be attributable to its porous structure which provides a large surface area and many more activated sites for hydrazine electrooxidation.

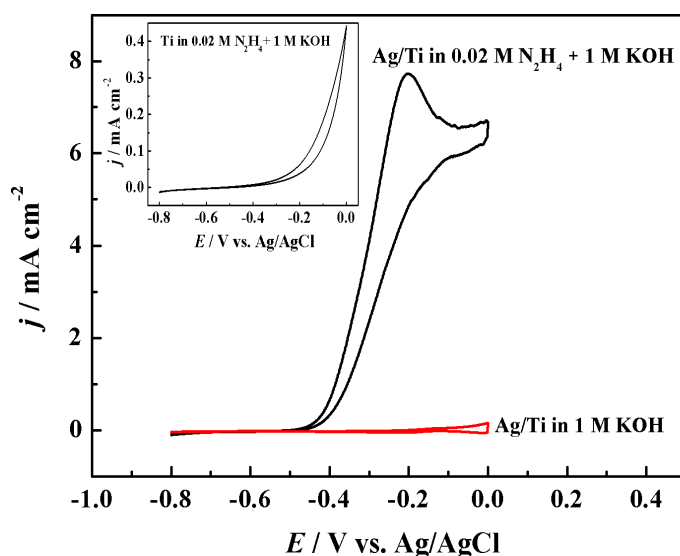


Figure 3. Cyclic voltammograms obtained on the Ag/Ti in 1.0 M KOH without and with $0.02 \text{ M N}_2\text{H}_4\cdot\text{H}_2\text{O}$ at 10 mV s^{-1} . Inset: cyclic voltammogram on the Ti substrate in $0.02 \text{ M N}_2\text{H}_4\cdot\text{H}_2\text{O} + 1.0 \text{ M KOH}$ at 10 mV s^{-1} .

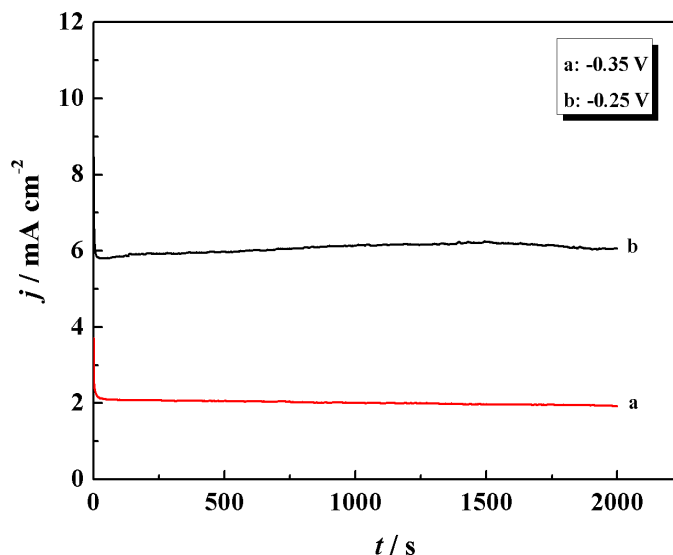


Figure 4. Chronoamperograms obtained on the sample at varying applied potentials in 0.02 M $\text{N}_2\text{H}_4\cdot\text{H}_2\text{O}$ + 1.0 M KOH.

Figure 4 shows the chronoamperometric curves obtained on the sample at varying applied potentials in 0.02 M $\text{N}_2\text{H}_4\cdot\text{H}_2\text{O}$ + 1.0 M KOH. With an augmented potential, the current density increased. The reason for this result was that higher potential will lead to a higher overpotential and faster reaction rate. The current density at each potential reached a steady state within the initial several seconds and then almost did not vary in the surplus time, indicating that the Ag/Ti electrode possessed an eminent electrocatalytic stability for hydrazine electrooxidation.

Preliminary research about the electrocatalytic character of the resulting sample toward N_2H_4 electrooxidation was conducted using a series of cyclic voltammetric curves tested at varying sweep rates in 0.02 M $\text{N}_2\text{H}_4\cdot\text{H}_2\text{O}$ + 1.0 M KOH, presented in Fig. 5. As observed, the peak current density owing to hydrazine electrooxidation became larger and the correspondent potential became more positive when the sweep rate increased gradually, showing that hydrazine electrooxidation occurring at the sample has irreversible characteristics. The increase in sweep rate can bring about a reduction in diffusion depth, weakened concentration polarization and increased peak current density. As the precondition semi-infinite linear diffusion implies, the relation of i_p and $v^{1/2}$ is written as the following formula (Eq. (1)) [22].

$$i_p = (3 \times 10^5) n (\alpha n_a)^{1/2} A C_0 D_0^{1/2} v^{1/2} \quad (1)$$

In the above formula, i_p represents the peak current density; n represents the electron transfer number for hydrazine electrooxidation reaction; α represents the charge transfer coefficient; n_a represents the electron transfer number of rate-determining step for hydrazine electrooxidation reaction; C_0 represents hydrazine concentration; A represents the Ag/Ti electrode area; D_0 represents the diffusion coefficient of hydrazine; $v^{1/2}$ represents the square root of sweep rate. When C_0 keeps unchangeably, i_p varies directly with $v^{1/2}$. When $v^{1/2}$ keeps unchangeably, i_p varies directly with C_0 , showing the reaction is a diffusion-limited process. As evidenced by a satisfactory linear relationship between i_p and $v^{1/2}$ (inset of Fig. 5), hydrazine electrooxidation reaction at the Ti foil supported Ag electrode follows a diffusion control mechanism.

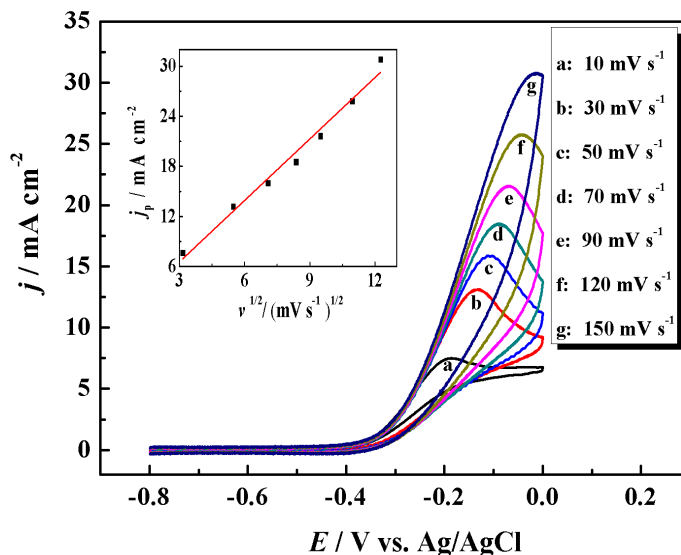


Figure 5. A series of cyclic voltammetric curves obtained on the sample at varying sweep rates in 0.02 M N₂H₄·H₂O + 1.0 M KOH. Inset: plot of i_p versus $v^{1/2}$.

Figure 6 gives a series of cyclic voltammograms on the sample in 1.0 M KOH and varying concentrated N₂H₄·H₂O at 10 mV s⁻¹. Hydrazine electrooxidation reaction became faster as hydrazine concentration increased. The logarithm of current density at -0.21 V ($\log j$) was plotted versus the logarithm of hydrazine concentration ($\log C$), exhibited in the inset. A linear relation of $\log j$ with $\log C$ was observed and the reaction order n was got from the line slope on the basis of Equation (2) [38]. The slope of the line was 0.9, showing that hydrazine electrooxidation reaction on the sample fits first-order kinetics well relative to hydrazine.

$$n_1 = \left(\frac{\partial \log j}{\partial \log C_i} \right)_{E,C_j} \tag{2}$$

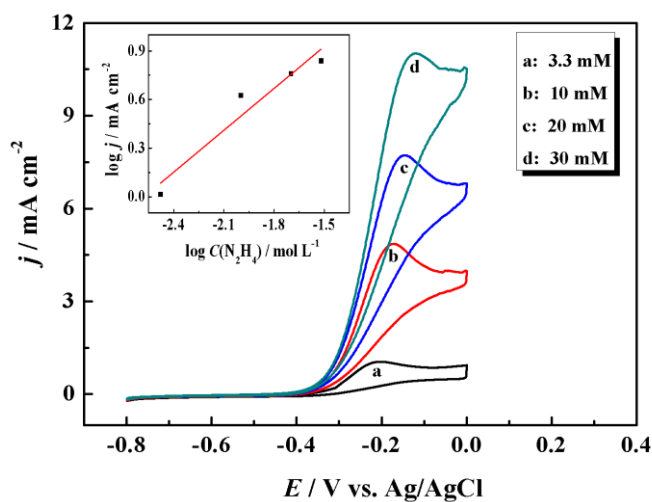


Figure 6. A series of cyclic voltammograms on the sample in 1.0 M KOH and varying concentrated N₂H₄·H₂O at 10 mV s⁻¹. Inset: plot of $\log j$ versus $\log C$.

Hydrazine electrooxidation reaction rate is dependent on temperature. Therefore, in order to discuss the temperature influence on the electrocatalytic activity, the cyclic voltammograms at various temperatures were carried out, as shown in Fig. 7. A temperature enhancement caused a gradual increase in the peak current density owing to hydrazine electrooxidation and a shift of the correspondent peak potential in negative direction, indicating that high temperature is favorable for elevating the electrocatalytic performance. The value of the apparent activation energy (E_a) for hydrazine electrooxidation reaction was determined from the plot of $\ln j$ versus $1/T$ based on the following Arrhenius equation (Eq. (3)) [22,39].

$$\ln j = -E_a/RT + \ln A \quad (3)$$

In the above equation, $\ln j$ represents the logarithm of current density at a given potential; T represents absolute temperature; A represents preexponential factor; R represents molar gas constant. The linear plots of $\ln j$ at different given potentials against $1/T$ were drawn, exhibited in the inset. From the slope of the correspondent plot, the apparent activation energies at -350 mV, -300 mV and -250 mV were calculated as 21.6, 19.7 and 14.6 kJ mol⁻¹, respectively. As shown from the above data that, the more positive the potential was, the lower the E_a value was. This suggested that the hydrazine electrooxidation reaction at the porous Ag/Ti electrode had a faster reaction kinetics at a more positive potential. In addition, E_a for hydrazine electrooxidation at the sample is much lower in comparison with that at the Ag/CFC electrode with a microspheric structure previously prepared by our team [40], showing the superiority of the highly porous structure.

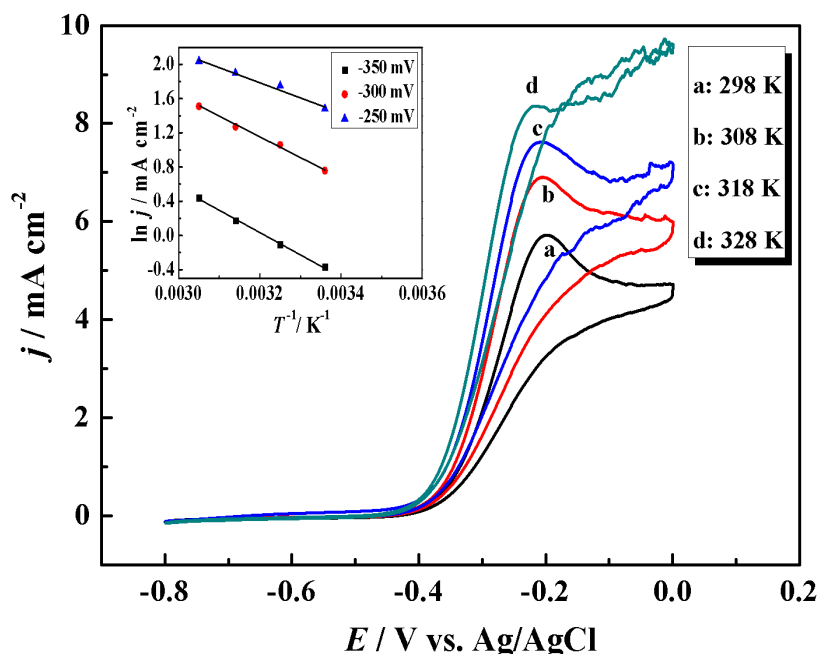


Figure 7. A series of cyclic voltammetric curves obtained on the sample at varying temperatures in 0.02 M N₂H₄·H₂O + 1.0 M KOH at 10 mV s⁻¹. Inset: plots of $\ln j$ at varying given potentials versus $1/T$.

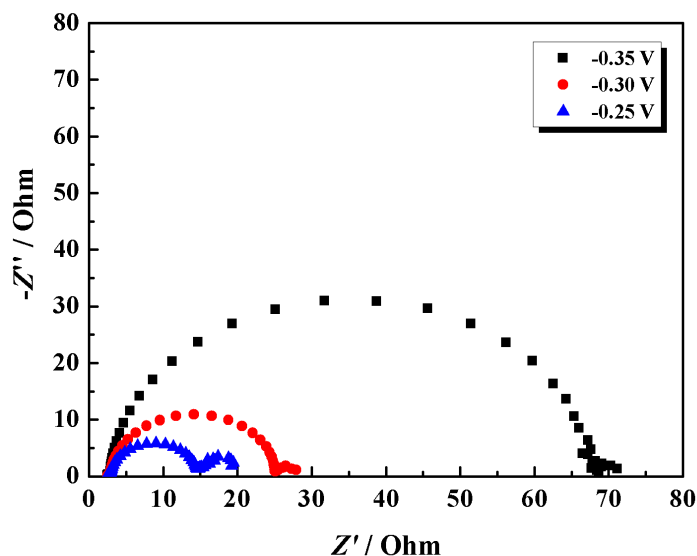
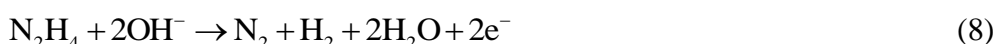
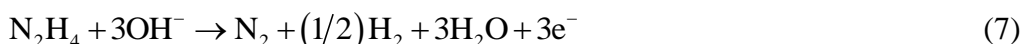


Figure 8. EIS curves of the sample at varying applied potentials in 0.02 M $\text{N}_2\text{H}_4 \cdot \text{H}_2\text{O}$ + 1.0 M KOH.

Figure 8 shows the EIS curves of the sample at varying applied potentials in 0.02 M $\text{N}_2\text{H}_4 \cdot \text{H}_2\text{O}$ + 1.0 M KOH. A depressed semicircle at higher frequencies was observed in the EIS curves at varying potentials. The hydrazine electrooxidation reaction resistance, estimated from the semicircle diameter, decreased with an increased applied potential, suggesting that hydrazine electrooxidation reaction was faster at a more positive potential. The impedance spectra presented only a few scattered points at lower frequencies, possibly because the release of gases generated from hydrazine electrooxidation severely agitated the electrolyte and reduced the effect of concentration polarization.

N_2H_4 is electrooxidized to generate nitrogen via two different pathways [18]: the first is a direct electrooxidation process according to Equation 4; the other is an indirect electrooxidation process, in which hydrogen formed by the decomposition of N_2H_4 (Eq. (5)) is electrooxidized in basic medium to produce water (Eq. (6)). Although the two pathways have different mechanisms, they share the same total reaction equation and achieve a four-electron oxidation. However, in real applications, N_2H_4 electrooxidation may occur through other modes (Eq. (7)-(8)), and achieve three-electron, two-electron oxidation [41], respectively, indicating that N_2H_4 is not completely oxidized and N_2H_4 usage efficiency is low.



Based on Faraday's law [41], the dependent relationships of the theoretical gas generating rate with applying fixed current density for 4e, 3e and 2e N_2H_4 oxidation reactions were obtained, displayed in Fig. 9. The gas generating rates of N_2H_4 electrooxidation on the Ag/Ti sample at varying current densities were measured by means of the drainage approach, marked with a triangle symbol

and shown in Fig. 9. As observed, N_2H_4 electrooxidation on the Ag/Ti sample abided by a four-electron oxidation mechanism.

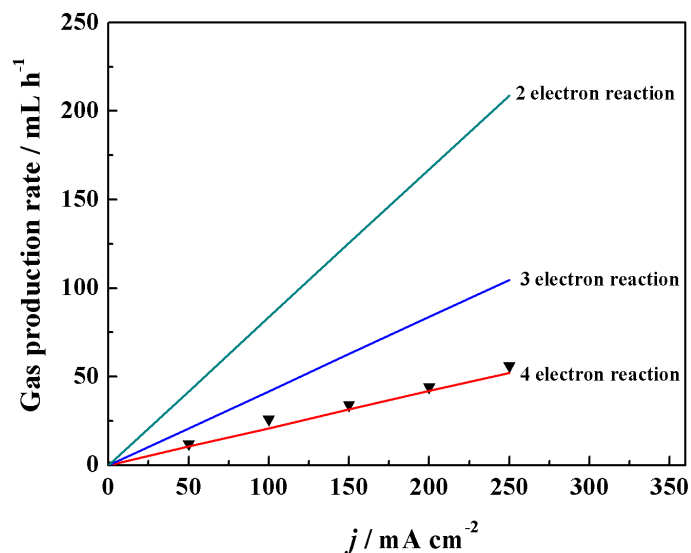


Figure 9. Gas generation rates of N_2H_4 electrooxidation on the sample at varying current densities.

4. CONCLUSIONS

A porous silver film was successfully deposited on Ti foil via a hydrogen bubbles template method. The results from electrochemical tests showed that the Ag/Ti electrode exhibited superior electrocatalytic activity, excellent stability, low charge transfer resistance and low apparent activation energy. This may be due to the precious porous structure of the electrode, which gives the electrode satisfying mass transfer characteristic and improves the electrolyte-electrode interface reaction rate. More importantly, the structure can favor the rapid release of gaseous products and prevent them from occupying the active sites. It was found that the hydrazine electrooxidation reaction on the Ag/Ti agrees with first-order kinetics relative to hydrazine and occurs more easily at a more positive potential. Hydrazine electrooxidation follows a four-electron oxidation mechanism, suggesting a high fuel usage efficiency. The porous Ag/Ti electrode with excellent electrocatalytic activity and stability was fabricated easily and may be a promising catalyst to catalyze hydrazine electrooxidation.

ACKNOWLEDGEMENTS

This work was supported by the Science and Technology Research Project of Department of Education of Heilongjiang Province (12543043) and the Youth Doctor Scientific Research Fund Project of Harbin University (HUDF201703).

References

1. H. -W. Wu, *Appl. Energy*, 165 (2016) 81.

2. D. Banham, S. Ye, K. Pei, J. -I. Ozaki, T. Kishimoto and Y. Imashiro, *J. Power Sources*, 285 (2015) 334.
3. Y. Yi, B. -D. Lee, S. -K. Kim, D. -H. Jung, E. -M. Jung, S. -M. Hwang, S. -Y. Choi and D. -H. Peck, *Int. J. Electrochem. Sci.*, 11 (2016) 5909.
4. A. Yousef, R. M. Brooks, M. M. El-Halwany, M. A. Abdelkareem, J. A. Khamaj, M. H. EL-Newehy, N. A. M. Barakat and H. Y. Kim, *Int. J. Electrochem. Sci.*, 10 (2015) 7025.
5. V. Livshits and E. Peled, *J. Power Sources*, 162 (2006) 1187.
6. C. Liu, M. Chen, C. Y. Du, J. Zhang, G. P. Yin, P. F. Shi and Y. R. Sun, *Int. J. Electrochem. Sci.*, 7 (2012) 10592.
7. P. -Y. Olu, N. Job and M. Chatenet, *J. Power Sources*, 327 (2016) 235.
8. S. M. M. Ehteshami, M. Asadnia, S. N. Tan and S. H. Chan, *J. Power Sources*, 301 (2016) 392.
9. A. Serov, M. Padilla, A. J. Roy, P. Atanassov, T. Sakamoto, K. Asazawa and H. Tanaka, *Angew. Chem. Int. Edit.*, 53 (2014) 10336.
10. X. Liu, Y. X. Li, N. Chen, D. Y. Deng, X. X. Xing and Y. D. Wang, *Electrochim. Acta*, 213 (2016) 730.
11. X. L. Wang, Y. X. Zheng, M. L. Jia, L. S. Yuan, C. Peng and W. H. Yang, *Int. J. Hydrogen Energy*, 41 (2016) 8449.
12. Y. Y. Ma, H. Wang, J. Key, S. Ji, W. Z. Lv and R. F. Wang, *J. Power Sources*, 300 (2015) 344.
13. T. Koderu, M. Honda and H. Kita, *Electrochim. Acta*, 30 (1985) 669.
14. F. M. Li, Y. G. Ji, S. M. Wang, S. N. Li and Y. Chen, *Electrochim. Acta*, 176 (2015) 125.
15. P. V. Dudin, P. R. Unwin and J. V. Macpherson, *Phys. Chem. Chem. Phys.*, 13 (2011) 17146.
16. G. W. Yang, G. Y. Gao, C. Wang, C. L. Xu and H. L. Li, *Carbon*, 46 (2008) 747.
17. T. -Y. Jeon, M. Watanabe and K. Miyatake, *Acs Appl. Mater. Interfaces*, 6 (2014) 18445.
18. J. Sanabria-Chinchilla, K. Asazawa, T. Sakamoto, K. Yamada, H. Tanaka and P. Strasser, *J. Am. Chem. Soc.*, 133 (2011) 5425.
19. S. Hussain, K. Akbar, D. Vikraman, M. A. Shehzad, S. Jung, Y. Seo and J. Jung, *RSC Adv.*, 20 (2015) 15374.
20. B. Dong, W. H. Hu, X. Y. Zhang, J. Wang, S. S. Lu, X. Li, X. Shang, Y. R. Liu, G. Q. Han, Y. M. Chai and C. G. Liu, *Mater. Lett.*, 189 (2017) 9.
21. C. G. He, Z. X. Liu, Y. Lu, L. P. Huang and Y. K. Yang, *Int. J. Electrochem. Sci.*, 11 (2016) 9566.
22. M. Hosseini and M. M. Momeni, *J. Mater. Sci.* 45 (2010) 3304.
23. D. K. Sharma, A. Ott, A. P. O'Mullane and S. K. Bhargava, *Colloids Surf. A Physicochem. Eng. Asp.*, 386 (2011) 98.
24. W. -H. Hu, X. Shang, X. -Y. Zhang, J. Wang, B. Dong, X. Li, Y. -R. Liu, G. -Q. Han, Y. -M. Chai and C. -G. Liu, *Mater. Lett.*, 185 (2016) 346.
25. F. Guo, D. X. Cao, M. M. Du, K. Ye, G. L. Wang, W. P. Zhang, Y. Y. Gao and K. Cheng, *J. Power Sources*, 307 (2016) 697.
26. H. Wu, N. Du, J. Z. Wang, H. Zhang and D. Yang, *J. Power Sources*, 246 (2014) 198.
27. M. -G. Jeong, K. Zhuo, S. Cherevko, W. -J. Kim and C. -H. Chung, *J. Power Sources*, 244 (2013) 806.
28. M. Chen, C. J. Hou, D. Q. Huo, H. B. Fa, Y. N. Zhao and C. H. Shen, *Sensor. Actuat. B-Chem.*, 239 (2017) 421.
29. H. C. Shin, J. Dong and M. Liu, *Adv. Mater.*, 15 (2003) 1610.
30. H. C. Shin and M. L. Liu, *Chem. Mater.*, 16 (2004) 5460.
31. S. Aich, M. K. Mishra, C. Sekhar, D. Satapathy and B. Roy, *Mater. Lett.*, 178 (2016) 135.
32. S. Cherevko, X. L. Xing and C. -H. Chung, *Electrochem. Commun.*, 12 (2010) 467.
33. R. Ojani, A. Alinezhad, M. J. Aghajani and S. Safshekan, *J. Solid State Electrochem.*, 19 (2015) 2235.
34. L. Luo, Z. Y. Duan, H. Li, J. Kim, G. Henkelman and R. M. Crooks, *J. Am. Chem. Soc.*, 139 (2017) 5538.

35. P. Kunal, H. Li, B. L. Dewing, L. Zhang, K. Jarvis, G. Henkelman and S. M. Humphrey, *ACS Catal.*, 6 (2016) 4882.
36. J. K. Nørskov, J. Rossmeisl, A. Logadottir and L. Lindqvist, *J. Phys. Chem. B*, 108 (2004) 17886.
37. A. J. Ahern, L. C. Nagle and L. D. Burke, *J. Solid State Electrochem.*, 6 (2002) 451.
38. D. X. Cao, L. M. Sun, G. L. Wang, Y. Z. Lv and M. L. Zhang, *J. Electroanal. Chem.*, 621 (2008) 31.
39. K. Ghanbari, *Synth. Met.*, 195 (2014) 234.
40. R. Liu, K. Ye, Y. Y. Gao, W. P. Zhang, G. L. Wang and D. X. Cao, *Electrochim. Acta*, 186 (2015) 239.
41. W. X. Yin, Z. P. Li, J. K. Zhu and H. Y. Qin, *J. Power Sources*, 182 (2008) 520.

© 2017 The Authors. Published by ESG (www.electrochemsci.org). This article is an open access article distributed under the terms and conditions of the Creative Commons Attribution license (<http://creativecommons.org/licenses/by/4.0/>).